

# Active Vibration Control in a Rotor System by an Active Suspension with Linear Actuators

M. Arias-Montiel<sup>\*1</sup>, G. Silva-Navarro<sup>2</sup> and A. Antonio-García<sup>3</sup>

<sup>1,3</sup> Instituto de Electrónica y Mecatrónica  
Universidad Tecnológica de la Mixteca  
Huajuapán de León, Oaxaca, México

\*mam@mixteco.utm.mx

<sup>2</sup> Departamento de Ingeniería Eléctrica – Sección de Mecatrónica  
Centro de Investigación y de Estudios Avanzados del Instituto Politécnico Nacional  
México, D. F., México

## ABSTRACT

In this paper the problem of modeling, analysis and unbalance response control of a rotor system with two disks in an asymmetrical configuration is treated. The Finite Element Method (FEM) is used to get the system model including the gyroscopic effects and then, the obtained model is experimentally validated. Rotordynamic analysis is carried out using the finite element model obtaining the Campbell diagram, the natural frequencies and the critical speeds of the rotor system. An asymptotic observer is designed to estimate the full state vector which is used to synthesize a Linear Quadratic Regulator (LQR) to reduce the vibration amplitudes when the system passes through the first critical speed. Some numerical simulations are carried out to verify the closed-loop system behavior. The active vibration control scheme is experimentally validated using an active suspension with electromechanical linear actuators, obtaining significant reductions in the resonant peak.

Keywords: Active vibration control, rotor system, active suspension.

## 1. Introduction

Rotating machinery plays an important role in modern industry due to the wide range of applications of these kind of machines (i.e. turbomachinery, compressors, generators, etc.). The presence of mechanical vibrations is an inherent phenomenon in rotating machinery. Mass unbalance and dynamic interaction between the stator and rotating parts are the main causes for vibrations. The trend in industry has been to move towards high speed, high power, lighter and more compact machinery, which has resulted in machines operating above their first critical speed and increasing the vibrations problem [1-4]. In spite of the fact that the total elimination of the mass unbalance is impossible, it is very important to control the vibration amplitudes within acceptable limits for a safe operation of the machines. To do this, machinery designers have to understand and predict the rotordynamic behavior of machinery taking advantage of the improvements in computing technologies and modeling techniques, nowadays finite element techniques are widely used to model and to

analyze rotor systems (see e.g. [2,3,5,6,7]). However, we must keep in mind that any model is only an approximation of a real system and its experimental validation has to carry out. The prototypes in laboratories are very important in the study of rotordynamics because by these, the analytical models and the control schemes proposed can be experimentally validated.

Nowadays, many machines must operate to high rotating speeds which yields a supercritical operation, that is, during the running up the machine has to cross one or more critical speeds causing large vibration amplitudes and more complex dynamic effects [2,3]. Some authors have presented important results about rotordynamics analysis such as [8,9], or fault diagnosis in rotor-bearing systems [10-12], but they do not include control schemes to attenuate the vibration amplitudes. On the other hand, rotating machines increasingly incorporate transducers, actuators and control systems, in order to attenuate vibration amplitudes, to improve the machines performance

and to extend their useful life. One of the most important issues of this tendency is the use of active bearings. Active vibration control has been an area of theoretical and experimental research in rotordynamics, providing many advantages for the attenuation of vibration amplitude, during run-up and coast-down through critical speeds, and minimization of sudden transient behavior due to rotor unbalance or parametric uncertainty. In literature many control strategies to reduce the unbalance response in the classical Jeffcott rotor have been published, but using very simple models [13,14]. Other authors have proposed the use of active bearings to control the unbalance response in rotor systems with more than a disk. Nicoletti and Santos [15] show a methodology to design an active control of vibrations in a rotor system using actively lubricated bearings, they employ two control strategies, in the first one the control system reduces the vibration amplitudes at the desired position of the shaft, at the expense of increasing displacement at the ends of the flexible rotor and, in the second one, significant reduction of vibration amplitude along the whole rotor is achieved, and finally, they found that the actuator must operate in a linear range and the excitation frequency must be less than the natural frequency of the servo valve, otherwise, the control system does not properly operate, the results are presented by numerical simulations. Active Magnetic Bearings (AMB) and piezoelectric actuators are other devices used to control actively vibrations in rotor systems. Bi et al. [16] propose an automatic learning control for unbalance compensation using two AMB in a small rotor of around 1.5kg obtaining an important reduction in vibration amplitudes crossing the first critical speed. Couzon and Der Hagopian [17] combine neural networks to identify and fuzzy logic to control the flexible modes of a rotor suspended on active magnetic bearings and working under the first critical speed, they obtain the system finite element model by software to design the control scheme and then, they validate experimentally this control law proving that it is possible to use artificial intelligence in the active control of a flexible structure. Lei and Palazzolo [18] present the design and analysis of a rotating system with magnetic bearings including dynamics, control and simulation results, by rotordynamic analysis they find that the first bending mode is above the maximum operating speed which permits the

controller design to ignore the flexible mode; they do not present experimental results, but they show the importance of a multidisciplinary design. Simoes et al. [19] show an active vibration control for unbalance compensation using piezoelectric actuators and show that important reductions in the vibration amplitudes are possible using active bearings with linear actuators. However, AMB and piezoelectric actuators are rather expensive, exhibit physical limitations and sometimes they are not easily available (see e.g. [20]). All of the works mentioned above use a reduced order model obtained by finite element techniques, but only some of them use experimental results to validate the mathematical models and control schemes.

In this work a reduced order model for a rotor system with two disks is obtained by the finite element method. The system model includes the gyroscopic effects and it is experimentally validated and used to get the Campbell diagram, the critical speeds and the mode shapes. An asymptotic observer is designed to estimate the full vector of system states and then, with the estimated states, a Linear Quadratic Regulator (LQR) with state feedback controller is synthesized to attenuate the resonant peak in vibration amplitudes when the rotor passes through the first critical speed. Some numerical simulations to validate the control scheme proposed are presented. The experimental test rig described in [21] was used to carry out some experiments to validate the closed loop system behavior. This experimental results show important reductions in the unbalance response of the overall system.

## 2. System modeling and analysis

### 2.1 Description and finite element model of the rotor system

First, we consider a rotor-bearing system shown in Figure 1. The rotor system is driven by an AC motor, which is connected to a steel shaft by a flexible couple. The shaft is supported by a traditional journal bearing on its ends. Two unbalanced disks are mounted in an asymmetrical way along the shaft, and the disks are fixed to the shaft by bridles. The motor and both bearings are fixed on a thick metallic base in order to give high stiffness to the system.

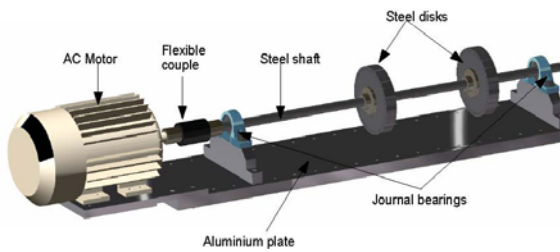


Figure 1. Rotor-bearing system.

In order to obtain a finite element model, the rotor system was divided in three elements and four nodes, one in each journal bearing and another one in each disk location. It is important to mention that such elements have different length. A finite element type Euler beam is considered with the following assumptions: the system is isotropic such as we analyze only a plane of motion, the shaft presents a linear elastic behavior and the disk masses are lumped in the corresponding nodes. This element has two degrees of freedom in each node, a radial displacement denoted by  $R_x$ , and an angle of deflection denoted by  $\beta_y$ . The mass, stiffness and gyroscopic matrices for this type of element are given in [3]. To assembly the mass and stiffness matrices, the consistent approach presented by Genta [22] was employed.

Considering the vector of generalized displacements

$$\mathbf{u} = [R_{x1} \quad \beta_{y1} \quad R_{x2} \quad \beta_{y2} \quad R_{x3} \quad \beta_{y3} \quad R_{x4} \quad \beta_{y4}]^T \quad (1)$$

we can obtain dynamics of undamped system behavior in free vibrations by

$$(\mathbf{M}_T + \mathbf{M}_R)\mathbf{u} + \Omega \mathbf{G}_{GYR} \mathbf{u} + \mathbf{K}\mathbf{u} = 0 \quad (2)$$

Where  $\mathbf{M}_T$  and  $\mathbf{M}_R$  are mass global matrices linked with translational and rotational inertia respectively,  $\mathbf{G}_{GYR}$  is the global gyroscopic matrix,  $\mathbf{K}$  is the global stiffness matrix and  $\Omega$  is the rotational speed.

When the boundary conditions are applied (rigid supports in shaft ends), the vector of generalized displacements becomes

$$\mathbf{u} = [\beta_{y1} \quad R_{x2} \quad \beta_{y2} \quad R_{x3} \quad \beta_{y3} \quad \beta_{y4}]^T \quad (3)$$

## 2.2 Natural frequencies and critical speeds

As the rotational speed appears explicitly in the equation of motion (Eq. 2), the natural frequencies  $\omega$  of the system depend on that rotational speed. When this occurs, the behavior of the system is summarized by a plot of the natural frequencies as functions of the rotational speed  $\Omega$ . Because in many cases the frequencies of the exciting forces depend on the speed, they can be reported on the same plot, obtaining the *Campbell diagram*.

In the particular case of the disturbance due to mass unbalance, the forcing frequency can be represented on the Campbell diagram by a straight line  $\omega = \Omega$ . The critical speeds occur when the frequency of the forcing function coincides with one of the natural frequencies of the system. It can be seen on the Campbell diagram by the intersection of the curves of the natural frequencies with those related with the forcing frequencies. The natural frequencies can be found as eigenvalues of the matrix (see [3]):

$$\begin{bmatrix} -\mathbf{M}^{-1}(\Omega \mathbf{G}_{GYR}) & -\mathbf{M}^{-1} \mathbf{K} \\ \mathbf{I} & 0 \end{bmatrix} \quad (4)$$

where  $\mathbf{M} = \mathbf{M}_T + \mathbf{M}_R$ .

The parameters used to obtain the Campbell diagram and for numerical simulation are presented in Table 1, which correspond with the physical prototype described in [21]. It is important to mention that the eccentricity parameters were experimentally estimated by peak peaking techniques.

In Figure 2 the Campbell diagram for the two first natural frequencies is depicted. We can observe two branches stemming from a same point, this point is a natural frequency at standstill and the branches can be interpreted as the frequencies of two circular whirling motions, one occurring in the same direction of the rotational speed (*forward whirling*) and another one in the opposite direction (*backward whirling*). If the natural frequencies are independent of the spin speed, the Campbell diagram is represented by a straight line parallel to the  $\Omega$  axis, as in the case in which the gyroscopic effects are neglected and the critical speeds coincide with the natural frequencies at a standstill.

Parameter	Value
Shaft density, $\rho$	$7850 \frac{\text{kg}}{\text{m}^3}$
Shaft diameter, $d$	0.020 m
Mass per length unit, $m$	$2.466 \frac{\text{kg}}{\text{m}}$
Disks mass, $m_{d1}, m_{d2}$	3.9 kg
Length, $L_1$	0.25 m
Length, $L_2$	0.35 m
Length, $L_3$	0.15 m
Young's modulus, $E$	211 GPa
Moment of inertia of shaft, $I$	$7.854 \times 10^{-9} \text{ m}^4$
Diametral moment of inertia per length unit of shaft, $j$	$6.1654 \times 10^{-5} \text{ kg} \cdot \text{m}$
Polar moment of inertia per length unit of shaft, $\bar{j}$	$1.2331 \times 10^{-4} \text{ kg} \cdot \text{m}$
Diametral moment of inertia disk, $J_d$	0.0057 $\text{kg} \cdot \text{m}^2$
Polar moment of inertia of disk, $\bar{J}_d$	0.0113 $\text{kg} \cdot \text{m}^2$
Eccentricity of disk 1, $a_1$	$7.3 \times 10^{-5} \text{ m}$
Eccentricity of disk 2, $a_2$	$22.2 \times 10^{-5} \text{ m}$

Table 1. System parameters.

The inclusion of gyroscopic effects in the model tends to increase the value of the forward critical speeds, as we can observe in the Campbell diagram.

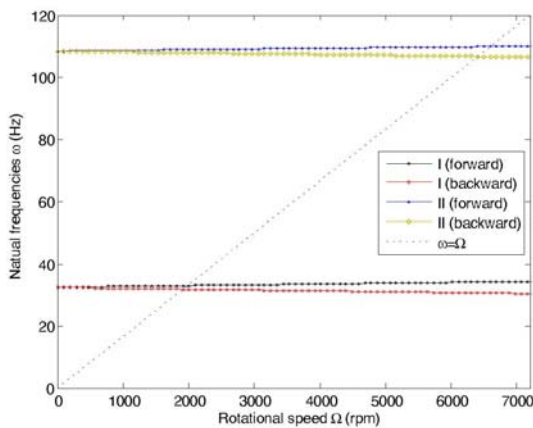


Figure 2. Campbell diagram.

The first two critical speed obtained by Figure 2 are  $\omega_1 = 33 \text{ Hz} = 1980 \text{ rpm}$  and  $\omega_2 = 109.8 \text{ Hz} = 6592 \text{ rpm}$ .

When the eigen-problem for matrix (4) is solved, complex numbers are obtained, the complex frequencies. The natural frequencies are given by the imaginary part and they are used to plot the Campbell diagram, while the real part represents the decay rate which can be used to prove system stability [3]. In Figure 3 the real part of the first two complex frequencies is plotted. We can observe negative values for decay rate which implies the system is stable for the range of rotational speed shown (30000 rpm).

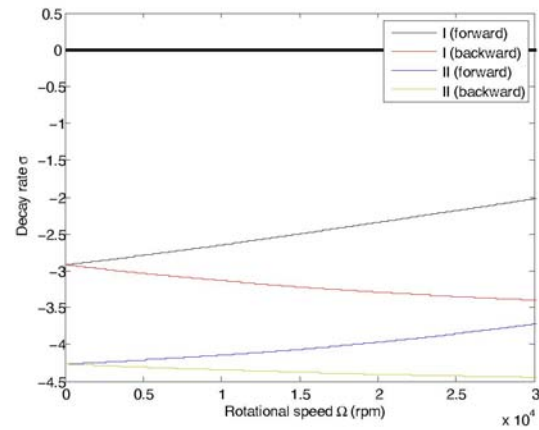


Figure 3. Decay rate.

### 2.3 Mode shapes

A modal system analysis was carried out in ANSYS finite element software to obtain the first two natural frequencies and their corresponding mode shapes. The mode shapes represent the deformation pattern induced in each natural frequency. In Figures 4 and 5, mode shapes for the first two natural frequencies are shown.

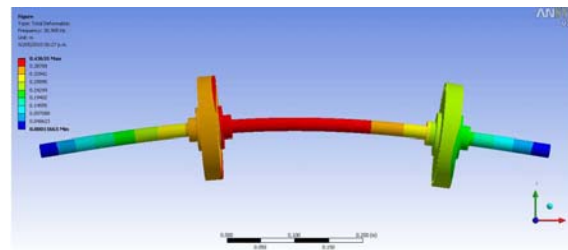


Figure 4. Modal shape related with the first natural frequency.

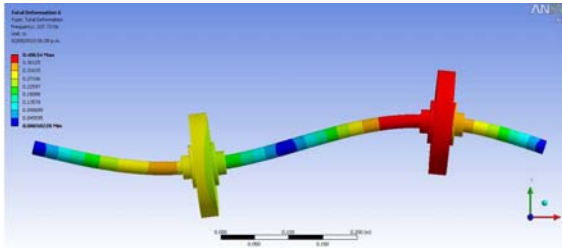


Figure 5. Modal shape related with the second natural frequency.

### 3. Experimental model validation

Validation of model is carried out by comparing simulation and experimental results in time and in frequency domains. Experimental data were obtained by proximity sensors in the test rig (shown in Figure 6) operating from 0 to 3000 rpm. System response in time is presented in Figure 7, where we can observe that the model reasonable tracks the experimental results.

Then, the Fast Fourier Transforms (FFT) of the data of Figure 7 were obtained in order to get the system frequency response, and these results are presented in Figure 8, where we can see that the resonant peak in simulation corresponds with the critical speed obtained by the Campbell diagram 33 Hz, while the resonant peak in experimental data is at 32.9 Hz, that is only 0.3 percent of difference.

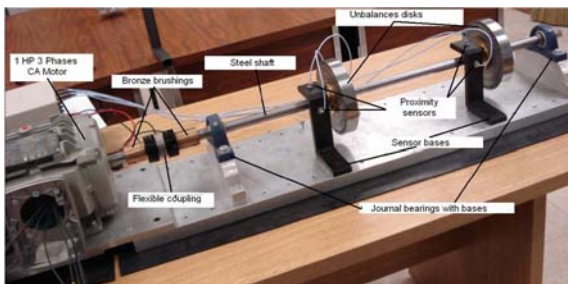


Figure 6. Experimental prototype with conventional bearings.

The amplitude peak observed in Figure 7 between 5 and 6 seconds may be caused by no modeled dynamic effects such as misalignment or bearing characteristics (they are not completely rigid). However, in the frequency response shown in Figure 8 does not present a resonant peak which means it is not a critical speed so that it will be neglected in the design of the active vibration control.

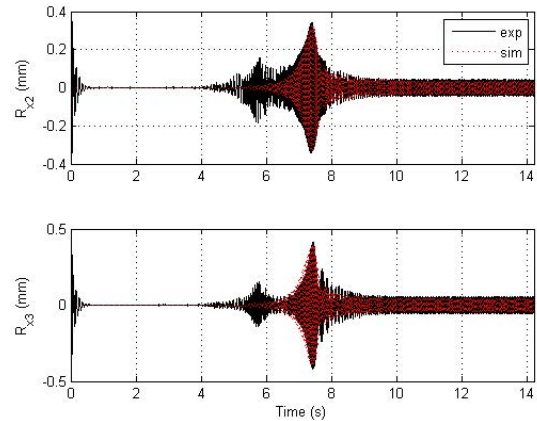


Figure 7. System response in time domain from 0 to 3000 rpm.

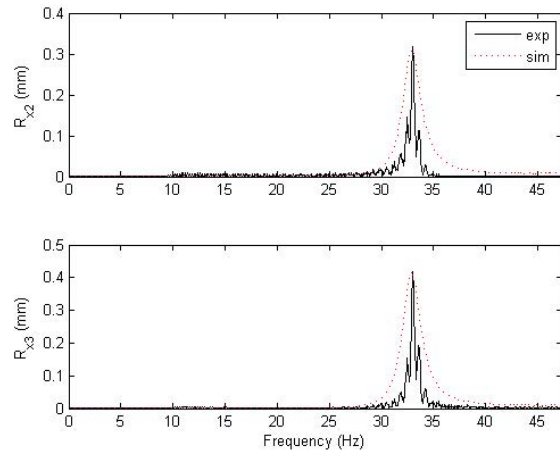


Figure 8. System response in time domain from 0 to 50 Hz.

### 4. System with active suspension

The system with the active suspension is presented in Figure 9.

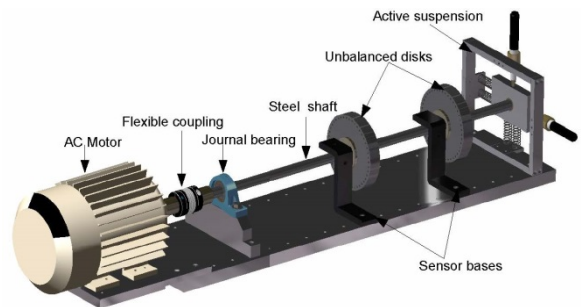


Figure 9. Rotor system with active suspension.

When the active suspension is incorporated to the system, one more degree of freedom must be added because the radial displacement at the right end is not constrained anymore, so the new generalized displacements are

$$\mathbf{u}_{cl} = [\beta_{y1} \quad R_{x2} \quad \beta_{y2} \quad R_{x3} \quad \beta_{y3} \quad R_{x4} \quad \beta_{y4}]^T \quad (5)$$

The rotor system dynamics is given by

$$\begin{aligned} M_{cl}\ddot{\mathbf{u}}_{cl} + (\Omega G_{cl} + D_{cl})\dot{\mathbf{u}}_{cl} + K_{cl}\mathbf{u}_{cl} \\ = \mathbf{b}f(t) + \mathbf{e}_1\varpi_1(t) + \mathbf{e}_2\varpi_2(t) \end{aligned} \quad (6)$$

where  $M_{cl}$ ,  $G_{cl}$ ,  $D_{cl}$  and  $K_{cl}$  are the mass, gyroscopic, damping and stiffness matrices, respectively, for the generalized displacements given by Eq. 5,  $f(t)$  is the force control input given by the linear actuators,  $\varpi_1$  and  $\varpi_2$  are the disturbance forces due to mass unbalance of disks,  $\mathbf{b}$ ,  $\mathbf{e}_1$  and  $\mathbf{e}_2$  are vectors indicating the degrees of freedom where the forces are acting.

The disturbance forces in transient state are

$$\varpi_1(t) = m_{d1}a_1\Omega^2\cos\varphi + m_{d1}a_1\Omega\sin\varphi \quad (7)$$

$$\varpi_2(t) = m_{d2}a_2\Omega^2\cos\varphi + m_{d2}a_2\Omega\sin\varphi \quad (8)$$

$$\text{with } \frac{d\varphi}{dt} = \Omega$$

It is important to remark that critical speeds change when the active suspension is incorporated to rotor system. Solving the eigen-problem with the new boundary conditions, the first critical speed is at 39.99 Hz = 2400 rpm.

## 5. Active control scheme

### 5.1 Controllability and observability

By defining the state vector  $\mathbf{z} = [\mathbf{u} \quad \dot{\mathbf{u}}]^T$ , dynamics system given by Eq. 6 can be described in state space form

$$\begin{aligned} \dot{\mathbf{z}} &= \mathbf{A}\mathbf{z} + \mathbf{B}f(t) + \mathbf{E}_1\varpi_1(t) + \mathbf{E}_2\varpi_2(t), \quad \mathbf{z} \in \mathfrak{R}^{14} \\ \mathbf{y} &= \mathbf{C}\mathbf{z}, \quad \mathbf{y} \in \mathfrak{R} \end{aligned} \quad (9)$$

with

$$\begin{aligned} \mathbf{A} &= \begin{bmatrix} 0 & \mathbf{I} \\ -\mathbf{M}_{cl}^{-1}\mathbf{K}_{cl} & -\mathbf{M}_{cl}^{-1}\mathbf{D}_{cl} \end{bmatrix}, \quad \mathbf{B} = \begin{bmatrix} 0 \\ \mathbf{M}_{cl}^{-1}\mathbf{b} \end{bmatrix}, \\ \mathbf{E}_1 &= \begin{bmatrix} 0 \\ \mathbf{M}_{cl}^{-1}\mathbf{e}_1 \end{bmatrix}, \quad \mathbf{E}_2 = \begin{bmatrix} 0 \\ \mathbf{M}_{cl}^{-1}\mathbf{e}_2 \end{bmatrix} \end{aligned} \quad (10)$$

$$\mathbf{C} = [0 \quad 1 \quad 0 \quad 0]$$

From the state space representation, controllability and observability matrices can be computed as

$$\mathbf{C}_{con} = [\mathbf{B} \quad \mathbf{A}\mathbf{B} \quad \mathbf{A}^2\mathbf{B} \quad \dots \quad \mathbf{A}^{13}\mathbf{B}] \quad (11)$$

$$\mathbf{O}_{obs} = [\mathbf{C} \quad \mathbf{A}\mathbf{C} \quad \mathbf{A}^2\mathbf{C} \quad \dots \quad \mathbf{A}^{13}\mathbf{C}]^T \quad (12)$$

which are of full rank, proving that the system of Eq. 9 is completely controllable from the control force  $f(t)$  and completely observable from the output  $R_{x2}$  (radial displacement of the first disk).

### 5.2 Asymptotic observer

In order to design a LQR controller based on a full state feedback, first, we design a full order asymptotic (Luenberger) observer (see e.g. [23]) to estimate the state vector considering that only the system output  $R_{x2}$  and the control input  $f(t)$  are available. The asymptotic observer is expressed by the dynamics

$$\begin{aligned} \dot{\hat{\mathbf{z}}} &= \mathbf{A}\hat{\mathbf{z}} + \mathbf{B}f(t) + \mathbf{E}_1\varpi_1(t) + \mathbf{E}_2\varpi_2(t) \\ &\quad + \mathbf{L}(\mathbf{y} - \hat{\mathbf{y}}), \quad \hat{\mathbf{z}} \in \mathfrak{R}^{14} \end{aligned} \quad (13)$$

$$\hat{\mathbf{y}} = \mathbf{C}\hat{\mathbf{z}}, \quad \hat{\mathbf{y}} \in \mathfrak{R}$$

where  $\hat{\mathbf{z}}$  is the estimated state vector and  $\mathbf{L}$  is a feedback gain matrix.

By defining the estimation error as

$$\tilde{\mathbf{z}} = \mathbf{z} - \hat{\mathbf{z}} \quad (14)$$

and properly selecting the matrix  $\mathbf{L}$ , the asymptotic convergence of the estimation error to zero can be guaranteed ( $\lim_{t \rightarrow \infty} \tilde{\mathbf{z}} = 0$ ), that is the estimated state  $\hat{\mathbf{z}}$  converges to the actual state  $\mathbf{z}$ . In order to satisfy this condition, the matrix  $\mathbf{L}$  is computed via pole-placement technique, such that the observer

dynamics described by Eq. 13 be sufficiently faster than the system dynamics given by Eq. 9.

### 5.3 LQR control

Using the estimated state vector given by the observer, a Linear Quadratic Regulator (LQR) based on full state feedback to attenuate the vibration amplitudes is proposed as follows

$$f(t) = -G\hat{z}(t) \quad (15)$$

where  $G$  is a gain matrix that minimizes a conventional LQR performance index with  $Q > 0$  and  $r > 0$  (see, e.g., [23]).

The linear electromechanical actuators are DC motors with geared reducer and a gear-screw type mechanism to transform the rotational in translational motion. Therefore, in order to take into account the actuators dynamics, the control force obtained by Eq. 15 is transformed and considered as a reference current for a PID current control for the linear actuator, whose output is the applied force to the system by the active bearing. A schematic diagram of the closed loop system is depicted in Figure 10.

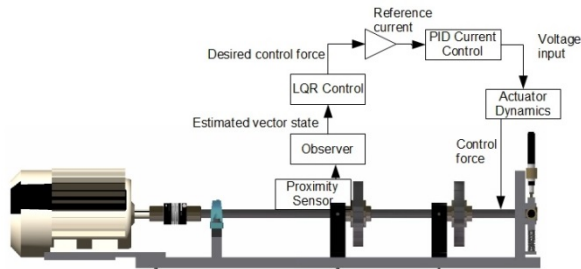


Figure 10. Schematic diagram of the closed loop system.

The actuator dynamics in state space is given by

$$\begin{aligned} \dot{w}_1 &= -\frac{R_a}{L_a} w_1 - \frac{k_{em}}{L_a} w_3 + \frac{1}{L_a} u \\ \dot{w}_2 &= w_3 \\ \dot{w}_3 &= \frac{k_T}{J_o} w_1 - \frac{b_o}{J_o} w_3 \\ T &= k_T w_1 \\ T_2 &= nT \\ F &= \frac{T_2}{r} \\ y_2 &= w_1 \end{aligned} \quad (16)$$

where  $w_1$  is the armature current,  $w_2$  the angular position,  $w_3$  the angular speed,  $R_a$  the armature resistance,  $L_a$  the armature inductance,  $k_{em}$  the back emf constant,  $u$  the input voltage,  $k_T$  the torque constant,  $J_o$  the rotor inertia,  $b_o$  the viscous damping coefficient,  $T$  the output torque,  $T_2$  the torque after the geared reducer,  $n$  the reduction constant,  $F$  the linear force provided by the actuator and  $r$  the radius in the gear-screw mechanism. The motor parameters are presented in Table 2. Some parameters were obtained from the manufacturer and other ones were estimated by experimental tests.

Parameter	Value
Armature resistance, $R_a$	19.8 $\Omega$
Armature inductance, $L_a$	250 $\mu\text{H}$
Back emf constant, $k_{em}$	$11.4 \times 10^{-3} \frac{\text{N} \cdot \text{s}}{\text{rad}}$
Rotor inertia, $J_o$	$6.5 \times 10^{-8} \text{kg} \cdot \text{m}^2$
Friction coefficient, $b_o$	$1.5 \times 10^{-6} \frac{\text{kg} \cdot \text{m}^2}{\text{s}}$
Reduction constant, $n$	69.12
Gear radius, $r$	0.00432 m

Table 2. Actuator parameters.

The PID current control action is obtained by

$$u = k_p (\hat{y}_2 - y_2) + k_d \frac{d(\hat{y}_2 - y_2)}{dt} + k_i \int_0^t (\hat{y}_2 - y_2) dt \quad (17)$$

with  $\hat{y}_2$  the reference current,  $k_p$ ,  $k_d$  and  $k_i$  the proportional, derivative and integral gains, respectively.

## 6. Numerical and experimental results

As we mentioned above, many rotating machines must operate to high rotating speeds which yields a supercritical operation, that is, during the running up the machine has to cross one or more critical speeds causing large vibration amplitudes [2,3]. The proposed controller was tuned to the critical case, when rotor system passes through the first resonant peak.

In Figures 11 and 12, the numerical results of the rotor system with the active suspension in open and in closed loop are presented. System

response is presented in time and in frequency domain from the standstill to operation speed (3000 rpm). A substantial reduction in the vibration amplitudes at the resonant peaks can be observed. In [24, 25], the response of the closed loop rotor system at constant speed is presented showing that the proposed control scheme can work in this condition too.

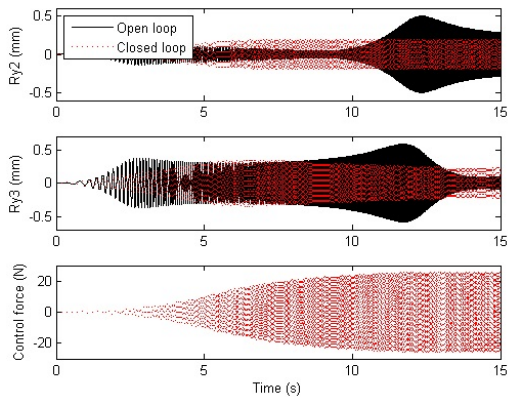


Figure 11. Numerical results in time domain.

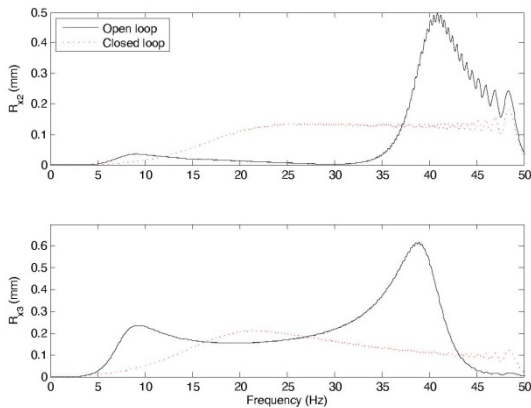


Figure 12. Numerical results in frequency domain.

In Figures 11 and 12 we can appreciate a magnification in closed loop system response in relation to open loop system in some low operation speeds, particularly at disk 1 location ( $R_{x2}$ ). This may be due to the fact that the controller was tuned for attenuation in the critical case (resonant peak corresponding to the first critical speed). Moreover, in a specific application, if those amplitudes were excessive, the controller would be triggered just before the system reaches the resonant condition to operate only in a time interval.

In order to validate the control scheme proposed, some experiments were carried out. In Figure 13 the test rig with the active suspension used to carry out the experiments is presented.



Figure 13. Experimental setup with active suspension.

The results are shown in Figures 14 and 15, in time and in frequency domain, respectively. The system operates from standstill to 3000 rpm. We can observe important reductions in the vibration amplitudes in both disks during the resonant peak.

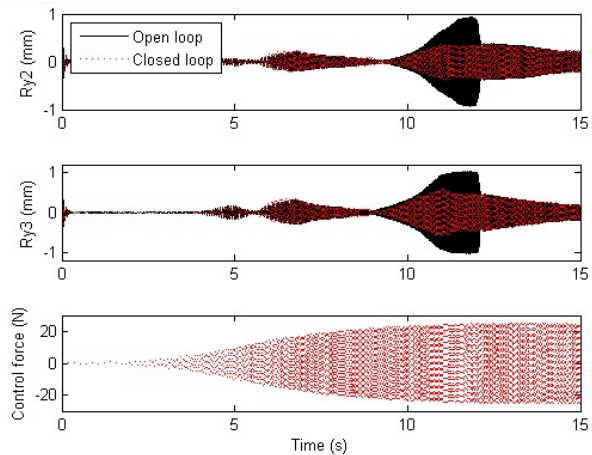


Figure 14. Experimental results in time domain.

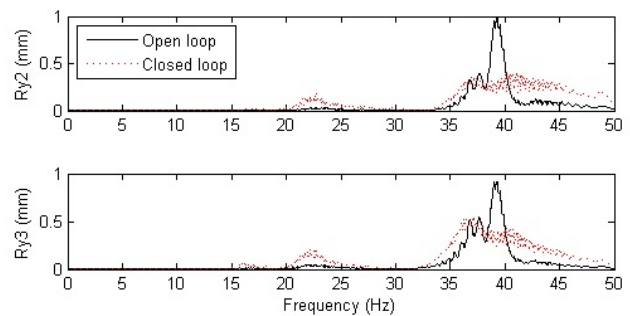


Figure 15. Experimental results in frequency domain.

## 7. Conclusions

In this work an active control scheme to reduce the unbalance response in a rotor system was presented. To do this a reduced order model for the rotor system was obtained by finite element techniques. This model includes the gyroscopic effects which allowed us to obtain the Campbell diagram to represent the dynamic behavior of the rotor system and it was experimentally validated. The inclusion of gyroscopic effects permits us to differentiate between the concepts of natural frequency and critical speed as well as to predict more precisely the resonance condition. Also, the decay rate plot was obtained from the finite element model, showing the system is stable in a wide range of rotational speed. The model was experimentally validated and used to design an asymptotic observer to estimate the full state vector in order to propose a linear quadratic regulator with full state feedback to attenuate the vibration amplitudes when the rotor pass through its first critical speed. This scheme was proved by numerical simulations. A novel active suspension using electromechanical actuators was designed and constructed in order to validate experimentally the closed loop system performance. Experimental results demonstrate reductions in the unbalance response about 66 percent in the first disk and 44 percent in the second one. Furthermore, the applied control efforts acquire reasonable values even when the system goes through its critical speed. It is important to mention that the power consumption of the actuator is around 2 W while the rotor system is driven by a motor of 1 HP.

## References

- [1] De Silva C., "Vibration Damping, Control and Design", Boca Raton, FL: CRC Press, 2007.
- [2] Friswell M.I. et al., "Dynamics of Rotating Machinery", New York, NY: Cambridge University Press, 2010.
- [3] Genta G., "Dynamics of Rotating Systems", New York, NY: Springer Science, 2005.
- [4] Vance J. et al, "Machinery Vibration and Rotordynamics", Hoboken, New Jersey: John Wiley & Sons, 2010.
- [5] Khoshravan M.R. and Paykani A., Design of a Composite Drive Shaft and its Coupling for Automotive Application, *J Appl Res Technol*, vol. 10, no. 6, pp. 826-834, 2012.
- [6] Vollan A. and Komzsis L., "Computational Techniques of Rotor Dynamics with the Finite Element Method", Boca Raton, FL: CRC Press, 2012.
- [7] Xian J. et al, Identification of Crack in a Rotor System Based on Wavelet Finite Element Method, *Finite Elem Anal Des*, vol. 43, no. 14, pp. 1068-1081, 2007.
- [8] Bucher I. and Ewins D. J., Modal Analysis and Testing of Rotating Structures, *Phil. Trans. R. Soc. Lon.*, vol. 359, no. 1778, pp. 61-96, 2001.
- [9] Suh J. H. et al, Modal Analysis of Asymmetric Rotor System with Isotropic Stator Using Modulated Coordinates, *J Sound Vib*, Vol. 284, no. 3-5, pp. 651-671, 2005.
- [10] Bachschmid N. et al, Identification of Multiple Faults in Rotor Systems, *J Sound Vib*, vol. 254, no. 2, pp. 327-366, 2002.
- [11] Lei Y. et al, Application of the EEMD Method to Rotor Fault Diagnosis in Rotating Machinery, *Mech Syst Signal Pr*, vol. 23, no. 4, pp. 1327-1338, 2009.
- [12] Saruhan H. et al, Vibration Analysis of Rolling Element Bearings Defects, *J Appl Res Technol*, vol. 12, no. 3, pp. 384-395, 2014.
- [13] Blanco-Ortega A. et al, Control de Vibraciones en Maquinaria Rotatoria, *Rev Iberoam Autom Inf Ind*, vol. 7, no. 4, pp. 36-43, 2010.
- [14] Zhou S. and Shi J., Active Balancing and Vibration Control of Rotating Machinery: A Survey, *Shock Vib Digest*, vol. 33, no. 4, pp. 361-371, 2001.

- [15] Nicoletti R. and Santos I. F., Control System Design for Flexible Rotors Supported by Actively Lubricated Bearings, *J Vib Control*, vol. 14, no. 3, pp. 347-374, 2008.
- [16] Bi C. et al, Automatic Learning Control for Unbalance Compensation in Active Magnetic Bearings, *IEEE Trans Magnetics*, vol. 41, no. 7, pp. 2270-2280, 2005.
- [17] Couzon P. Y. and Der Hagopian J., Neuro-Fuzzy Active Control of Rotor Suspended on Active Magnetic Bearings, *J Vib Control*, vol. 13, no. 4, pp. 365-384, 2007.
- [18] Lei S. and Palazzolo A., Control of Flexible Rotors Supported by Active Magnetic Bearings, *J Sound Vib*, vol. 314, no. 1-2, pp. 19-38, 2008.
- [19] Simoes R. C. et al, Active Vibration Control of a Rotor Using Piezoelectric Stack Actuators, *J Vib Control*, vol. 13, no. 1, pp. 45-64, 2007.
- [20] Schweitzer G. and Maslen E. H. (Eds), "Magnetic Bearings – Theory, Design and Application to Rotating Machinery", Berlin, Germany: Springer Verlag, 2010, pp. 151-165.
- [21] Arias-Montiel M. and Silva-Navarro G., "Design and Control of a Two Disks Asymmetrical Rotor System Supported by a Suspension with Linear Electromechanical Actuators", in Proceedings of 6th International Conference on Electrical Engineering, Computing Science and Automatic Control, Toluca, México, 2009, pp. 503-508.
- [22] Genta G., Consistent Matrices in Rotordynamics, *Meccanica*, vol. 20, no. 3, pp. 235-248, 1985.
- [23] Anderson B. D. O. and Moore J. B., "Optimal Control – Linear Quadratic Methods", New York, NY: Dover Publications, 2007, pp. 1-34.
- [24] Arias-Montiel M. et al, On-line algebraic identification of eccentricity parameters in active rotor-bearing systems, *Int J Mech Sci*, vol. 85, pp. 152-159, 2014.
- [25] Arias-Montiel M. and Silva-Navarro G., "Finite Element Modeling and Unbalance Compensation for a Two Disks Asymmetrical Rotor System", in Proceedings of 5th International Conference on Electrical Engineering, Computing Science and Automatic Control, Mexico City, México, 2008, pp. 386-391.